6-D Magnetic Localization and Orientation Method for an Annular Magnet Based on a Closed-Form Analytical Model

Shuang Song[1], Baopu Li[2,3], Wan Qiao[3], Chao Hu[4], Hongliang Ren[1], Haoyong Yu[1], Qi Zhang[3], Max Q.-H. Meng[5], and Guoqing Xu[3]

[1]Department of Biomedical Engineering, National University of Singapore, 119077 Singapore
[2]Department of Biomedical Engineering, College of Medicine, Shenzhen University, Shenzhen 518055, China
[3]Shenzhen Institutes of Advanced Technology, Chinese Academy of Sciences, Shenzhen 518055, China
[4]Ningbo Institute of Technology, Zhejiang University, Ningbo 315000, China
[5]Department of Electronic Engineering, Chinese University of Hong Kong, Hong Kong

Magnetic tracking technology is emerging to provide an occlusion-free tracking scheme for the estimation of full pose (position and orientation) of various instruments. This brings substantial benefits for intracorporeal applications, such as for tracking of flexible or wireless endoscopic devices, and thus is significant for further computer-assisted diagnosis, interventions, and surgeries. Toward efficient magnetic tracking, a 6-D magnetic localization and orientation method is proposed in this paper. An annular permanent magnet is mounted on the exterior surface of a capsule. With a magnetic sensor array, the magnetic field can be measured and the capsule's 3-D location and 3-D orientation information can be estimated based on proposed closed-form analytical model of annular magnet and particle swarm optimization algorithm. Magnetic dipole model and Levenberg–Marquardt algorithm are used to improve the speed and accuracy of estimation. Extensive simulation experiments show that the localization and orientation method works well with good position and orientation accuracy.

***Index Terms*— 6-D magnetic localization and orientation, annular magnet, computer-assisted interventions, particle swarm optimization (PSO), tracking.**

I. Introduction

MAGNETIC tracking technique uses one or more magnets as the excitation source, which generates a magnetic field that can be detected and measured by magnetic sensors. With these sensing signals, position and orientation can be estimated [1]–[4]. In contrast to other state-of-the-art tracking technologies such as mechanical optical tracking or ultrasonic tracking, magnetic tracking is emerging to provide an occlusion-free tracking scheme for the estimation of full pose (position and orientation) of various instruments [5]–[11]. Compared with optical tracking techniques, this occlusion-free feature brings substantial benefits for intracorporeal applications, which are typically lacking of direct line-of-sights between the base frames to the tracked targets [12]–[14].

Hence, efficient magnetic tracking techniques are significant for further development of computer-assisted diagnosis, interventions, and surgeries. For instance, there is demand for a clinical drive to track flexible cable-based or wireless endoscopic devices [12], [15], [16]. The cable-based endoscope has been widely used in traditional treatments over the past few decades and its localization is significant in navigated robotic surgeries. Compared with the cable-based endoscope, the wireless capsule endoscope has advantages including noninvasiveness and a direct view of the small intestine which is not reachable using traditional endoscopes [17]. Physicians can analyze status of the gastrointestinal (GI) tract by viewing the captured images after examination. However, the current wireless capsule endoscope technology still has some limitations. One drawback is that it cannot provide accurate location and orientation information of a capsule with respect to the patient's anatomy. Physicians sometimes require knowledge of accurate positional information of the pathological tissues to make a more accurate diagnosis so as to determine the need for further treatment or operation. Thus, the accurate location information is important for the diagnosis of GI pathologies [17]–[19].

In [20]–[24], the low-frequency ac signal is used to generate an electromagnetic field. This method can achieve high accuracy and fast estimation. However, for the tracking of an object inside the human body, using a method such as the wireless capsule endoscope, the wireless excitation technique is preferable. Because of application demands such as low power consumption and confined space, a small permanent magnet would be a better choice to serve as the excitation source instead of the magnetic coils excited by ac signals. Recently, many researchers have suggested that the magnetic localization and orientation technique can be employed to track short distance objects such as endoscopic devices inside human body [3], [11], [12], [22], [25]–[33]. This is because the human body has a magnetic permeability close to air, and the magnetic field generated by a small magnet is generally harmless to the human body. In addition, this magnetic technique is easier to implement compared with other techniques like computed tomography (CT), magnetic resonance imaging (MRI), and 3-D ultrasound.

Manuscript received November 20, 2013; revised January 28, 2014; accepted March 21, 2014. Date of publication April 3, 2014; date of current version September 9, 2014. Corresponding author: B. Li (e-mail: bpli@szu.edu.cn).

Color versions of one or more of the figures in this paper are available online at http://ieeexplore.ieee.org.

Digital Object Identifier 10.1109/TMAG.2014.2315592

With the magnetic localization method, some researchers have suggested using the superconducting quantum interference device (SQUID) technique to monitor the transit of magnetic markers [34]. However, SQUID requires cooling, and the measurements are usually performed in a magnetically shielded room. It is desirable to find a more convenient magnetic detection technique that can be realized in the normal environment. In [35], a 2-D array of hall sensors is used to track a permanent magnet with the size of 0.2 cm^3, but it can only acquire information in 5 degrees of freedom of the magnet and the detection distance is as short as 14 cm. In [36], the recursive Bayesian method and a tensor gradiometer are used to track a magnetic dipole. Using the magnetic dipole model, the rotation information about the magnetic moment cannot be calculated. A motion trajectory detecting method that permits the tracking of magnetic objects is presented in [37] using the magnetic flux density of a 3-D Hall probe. Generally, the aforementioned methods are all based on an internal magnetic source being sensed outside the human body. A different strategy to achieve real-time pose detection is based on an external permanent magnet (EPM) being sensed from inside the capsule [38], [39]. A localization method using an external rotating permanent magnet (RPM) has been proposed in [38]. Magnetic sensors are first placed inside the capsule. By measuring the maximum and minimum magnetic field values $B_{\max}$ and $B_{\min}$ from magnetic sensors, the capsule's position and orientation information can be estimated. In [39], a pose detection method that combines the use of magnetic sensors and a triaxial accelerometer was proposed. All these sensors are embedded in the capsule and an EPM is used as the magnetic source. Data from magnetic sensors and accelerometer are used to estimate the position and orientation parameters, respectively.

In [3], [22], [26], [28], and [29], we built a cubic magnetic sensor (Honeywell HMC1043) array to track small magnets. As shown in Fig. 1, it consists of four planes of magnetic sensors, which form a cubic inner space around 0.5 m $\times$ 0.4 m $\times$ 0.3 m. On each plane there are nine uniformly arranged three-axis magnetic sensors. The computer samples the signal by using a USB ADC (ZTIC-USB-7335) and then calculates the 3-D position parameters and 2-D orientation information of the magnets moving inside the sensor array. The system update rate is around 5 Hz and up to three magnets can be tracked at once.

In this paper, a 6-D localization and orientation method for wireless capsule endoscope based on an annular magnet is presented and discussed. As shown in Fig. 2, the magnet is mounted on the exterior surface of an endoscope. Compared with the cylindrical and rectangular magnet, the annular magnet can enlarge the usable space in the endoscope, while maintaining the strength of the magnetic field. There are two types of annular magnets, as shown in Fig. 2, magnet A and magnet B. They have the same shape and size, but different magnetic moment direction. Magnet A can only provide 5-D information: 3-D position and 2-D orientation. However, the rotation information about the magnetic moment cannot be determined. Magnet B can provide 6-D information: 3-D position and three rotation angles. The 6-D localization and orientation method proposed in this paper is based on the latter. The method includes three key parts: 1) a closed-form analytical model for the annular magnet field based on the electromagnetic field principle and the Biot–Savart Law; 2) a sensor array to measure the magnetic field strength generated by the annular magnet; and 3) an optimization algorithm to solve the equations based on the analytical model.

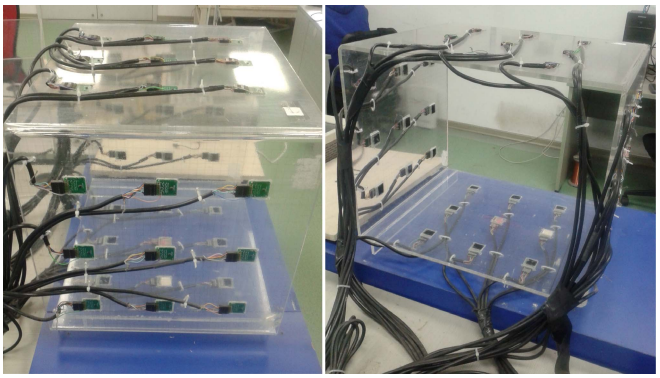

Fig. 1. Magnetic sensor array.

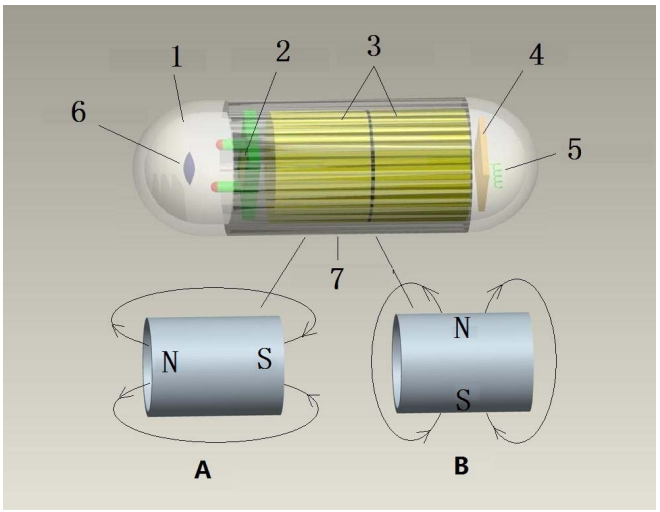

Fig. 2. Endoscope with annular magnet. 1: Optic dome; 2: CMOS imager; 3: battery; 4: RF emitter; 5: antenna; 6: optic lens; and 7: permanent magnet.

The organization of this paper is as follows. In Section II, the analytical model of annular magnet and the comparison with the magnetic dipole model will be discussed. In Section III, the localization and orientation method is presented in detail. In Section IV, the simulation results will be shown. Finally, conclusions will be made in Section V.

II. Closed-Form Analytical Model of Annular Magnet Field

The closed-form analytical model of the annular magnet field is based on the superposition principle and the Biot–Savart Law. As shown in Fig. 3, using the superposition principle, the magnetic field generated by an annular magnet is the same as that generated by two cylindrical magnets. The two cylindrical magnets share the same length and magnetic moment direction but different radius.

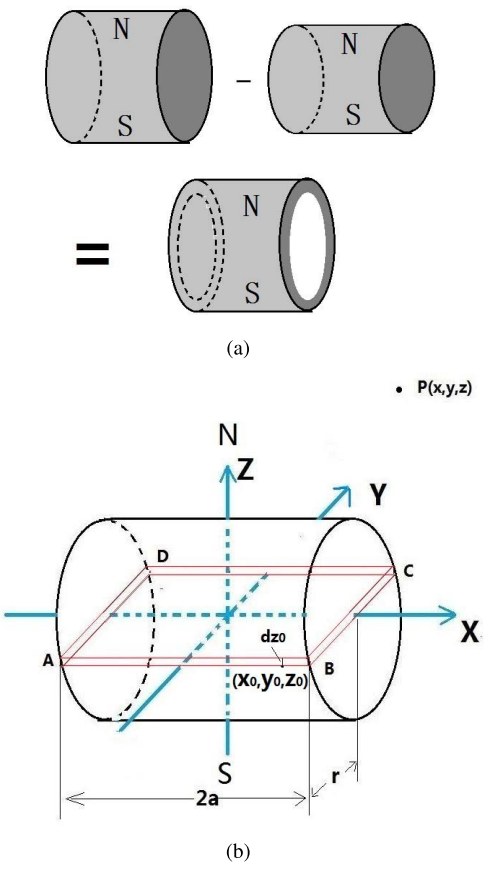

Fig. 3. Modeling of annular magnet. (a) Superposition principle. (b) Biot–Savart Law.

The subtraction of the magnetic field strength of the larger magnet with the smaller magnet will result in an equivalent annular magnet with the same magnetic moment direction and length. First, the closed-form analytical model of cylinder magnet will be presented.

A. Analytical Model of Cylinder Magnet Field

As shown in Fig. 3, the length of this cylindrical magnet is $2a$ and the radius is r. The magnetic moment direction is from Z_- to Z_+. Using the center of this magnet as the point of origin, the magnet's coordinates are established. With the Biot–Savart law, the magnetic field **dB** at the position $\mathbf{P}(x, y, z)$ generated by a surface current $\mathbf{I}_{ABCDA}$ with thickness of dz_0, can be calculated, with the current path being $A \rightarrow B \rightarrow C \rightarrow D \rightarrow A$. The surface current $\mathbf{I} = I\mathbf{dl}$ is shown in Fig. 3 using red lines, where $I = J_s dz_0$ is magnitude of current, **dl** is the direction of the current and J_s is the current density (A/m). Let (x_0, y_0, z_0) be a point on this current. The magnetic field at position **P** generated by the cylinder magnet can be estimated by

$$\mathbf{B} = \int_{-r}^{r} \mathbf{dB}. \tag{1}$$

The direction of current $\mathbf{I}_{AB}$ with segment AB is $(1, 0, 0)$. With the Biot–Savart law, the magnetic field strength generated by current $\mathbf{I}_{AB}$ can be calculated using the following equation:

$$\begin{aligned}\mathbf{dB_1} &= \frac{\mu_0}{4\pi}\frac{I\mathbf{dl}\times\mathbf{P_0}}{|\mathbf{P_0}|^3} \\ &= Kdz_0\int_{-a}^{a}\frac{\begin{vmatrix} i & j & k \\ 1 & 0 & 0 \\ x-x_0 & y-y_0 & z-z_0 \end{vmatrix}}{\left[(x-x_0)^2+(y-y_0)^2+(z-z_0)^2\right]^{3/2}}dx_0.\end{aligned} \tag{2}$$

Decomposing the above equation to three components, we have

$$\begin{cases} dB_{x1} = 0 \\ dB_{y1} = Kdz_0\int_{-a}^{a}\frac{(z_0-z)}{\left[(x-x_0)^2+(y-y_0)^2+(z-z_0)^2\right]^{3/2}}dx_0 \\ dB_{z1} = Kdz_0\int_{-a}^{a}\frac{(y-y_0)}{\left[(x-x_0)^2+(y-y_0)^2+(z-z_0)^2\right]^{3/2}}dx_0 \end{cases} \tag{3}$$

where $y_0 = -(r^2 - z_0^2)^{1/2}$, μ_0 is the permeability of vacuum in free space and $K = J_s\mu_0/4\pi$ is a constant determined based on the material of the magnet, and $\mathbf{P_0}$ is the vector from point (x_0, y_0, z_0) to point $\mathbf{P}(x, y, z)$.

For segment BC, the orientation of current $\mathbf{I}_{BC}$ is $(0, 1, 0)$. The magnetic field generated by current $\mathbf{I}_{BC}$ can be calculated with the subsequent equation

$$\begin{aligned}\mathbf{dB_2} &= \frac{\mu_0}{4\pi}\frac{I\mathbf{dl}\times\mathbf{P_0}}{|\mathbf{P_0}|^3} \\ &= Kdz_0\int_{-y'}^{y'}\frac{\begin{vmatrix} i & j & k \\ 0 & 1 & 0 \\ x-a & y-y_0 & z-z_0 \end{vmatrix}}{\left[(x-a)^2+(y-y_0)^2+(z-z_0)^2\right]^{3/2}}dy_0.\end{aligned} \tag{4}$$

Subsequently

$$\begin{cases} dB_{x2} = Kdz_0\int_{-y'}^{y'}\frac{(z-z_0)}{\left[(x-a)^2+(y-y_0)^2+(z-z_0)^2\right]^{3/2}}dy_0 \\ dB_{y2} = 0 \\ dB_{z2} = Kdz_0\int_{-y'}^{y'}\frac{-(x-a)}{\left[(x-a)^2+(y-y_0)^2+(z-z_0)^2\right]^{3/2}}dy_0 \end{cases} \tag{5}$$

where $y' = \sqrt{r^2 - z_0^2}$.

For current $\mathbf{I}_{CD}$, the direction is $(-1, 0, 0)$ and the magnetic field will be

$$\begin{aligned}\mathbf{dB_3} &= \frac{\mu_0}{4\pi}\frac{I\mathbf{dl}\times\mathbf{P_0}}{|\mathbf{P_0}|^3} \\ &= Kdz_0\int_{-a}^{a}\frac{\begin{vmatrix} i & j & k \\ -1 & 0 & 0 \\ x-x_0 & y-y_0 & z-z_0 \end{vmatrix}}{\left[(x-x_0)^2+(y-y_0)^2+(z-z_0)^2\right]^{3/2}}dx_0.\end{aligned} \tag{6}$$

Subsequently

$$\begin{cases} dB_{x3} = 0 \\ dB_{y3} = Kdz_0 \int_{-a}^{a} \frac{(z-z_0)}{\left[(x-x_0)^2+(y-y_0)^2+(z-z_0)^2\right]^{3/2}} dx_0 \\ dB_{z3} = Kdz_0 \int_{-a}^{a} \frac{(y_0-y)}{\left[(x-x_0)^2+(y-y_0)^2+(z-z_0)^2\right]^{3/2}} dx_0 \end{cases} \quad (7)$$

where $y_0 = \sqrt{r^2 - z_0^2}$.

For current $\mathbf{I}_{DA}$ with the direction $(0, -1, 0)$, the magnetic field will be

$$\mathbf{dB_4} = \frac{\mu_0}{4\pi} \frac{I\mathbf{dl} \times \mathbf{P_0}}{|\mathbf{P_0}|^3} = Kdz_0 \int_{-y'}^{y'} \frac{\begin{vmatrix} i & j & k \\ 0 & -1 & 0 \\ x+a & y-y_0 & z-z_0 \end{vmatrix}}{\left[(x+a)^2 + (y-y_0)^2 + (z-z_0)^2\right]^{3/2}} dy_0. \quad (8)$$

Subsequently

$$\begin{cases} dB_{x4} = Kdz_0 \int_{-y'}^{y'} \frac{-(z-z_0)}{\left[(x+a)^2+(y-y_0)^2+(z-z_0)^2\right]^{3/2}} dy_0 \\ dB_{y4} = 0 \\ dB_{z4} = Kdz_0 \int_{-y'}^{y'} \frac{(x+a)}{\left[(x+a)^2+(y-y_0)^2+(z-z_0)^2\right]^{3/2}} dy_0 \end{cases} \quad (9)$$

where $y' = \sqrt{r^2 - z_0^2}$.

With the superposition principle and the foregoing equations, the magnetic field $\mathbf{dB} = (dB_x, dB_y, dB_z)$ generated by surface current $\mathbf{I}_{ABCDA}$ can be calculated as follows:

$$(dB_x, dB_y, dB_z) = \left(\sum_{i=1}^{4} dB_{xi}, \sum_{i=1}^{4} dB_{yi}, \sum_{i=1}^{4} dB_{zi} \right). \quad (10)$$

Then (1) can be calculated as follows:

$$\mathbf{B} = (B_x, B_y, B_z) = \left(\int_{-r}^{r} dB_x, \int_{-r}^{r} dB_y, \int_{-r}^{r} dB_z \right). \quad (11)$$

To reduce the calculation overhead, the preceding double integral expressions can be simplified to integral expressions about z_0. A numerical integral evaluation is used for the calculation, and the final closed-form analytical expressions are as follows:

$$B_x = \frac{h}{6} \left[f_x(-r) + 4 \sum_{k=0}^{n-1} f_x \left(z_0 \left(k + \frac{1}{2} \right) \right) + 2 \sum_{k=0}^{n-1} f_x \left(z_0 (k) \right) + f_x(r) \right] \quad (12)$$

$$B_y = \frac{h}{6} \left[f_y(-r) + 4 \sum_{k=0}^{n-1} f_y \left(z_0 \left(k + \frac{1}{2} \right) \right) + 2 \sum_{k=0}^{n-1} f_y \left(z_0 (k) \right) + f_y(r) \right] \quad (13)$$

$$B_z = \frac{h}{6} \left[f_z(-r) + 4 \sum_{k=0}^{n-1} f_z \left(z_0 \left(k + \frac{1}{2} \right) \right) + 2 \sum_{k=0}^{n-1} f_z \left(z_0 (k) \right) + f_z(r) \right] \quad (14)$$

where $h = 2r/n$, $z_0(k) = -r + kh$, $z_0(k + 1/2) = z_0(k) + h/2$. $f_x(z_0)$, $f_y(z_0)$, $f_z(z_0)$ are shown in (15) as shown at the bottom of the page, and (16), (17) as shown at the bottom of the next page, respectively.

$$f_x(z_0) = K(z - z_0) \left(\frac{y + \sqrt{r^2 - z_0^2}}{\left[(x-a)^2 + (z-z_0)^2\right] \left[(x-a)^2 + (z-z_0)^2 + \left(y + \sqrt{r^2 - z_0^2} \right)^2 \right]^{\frac{1}{2}}} - \frac{y - \sqrt{r^2 - z_0^2}}{\left[(x-a)^2 + (z-z_0)^2\right] \left[(x-a)^2 + (z-z_0)^2 + \left(y - \sqrt{r^2 - z_0^2} \right)^2 \right]^{\frac{1}{2}}} - \frac{y + \sqrt{r^2 - z_0^2}}{\left[(x+a)^2 + (z-z_0)^2\right] \left[(x+a)^2 + (z-z_0)^2 + \left(y + \sqrt{r^2 - z_0^2} \right)^2 \right]^{\frac{1}{2}}} + \frac{y - \sqrt{r^2 - z_0^2}}{\left[(x+a)^2 + (z-z_0)^2\right] \left[(x+a)^2 + (z-z_0)^2 + \left(y - \sqrt{r^2 - z_0^2} \right)^2 \right]^{\frac{1}{2}}} \right) \quad (15)$$

By combining (12), (13), and (14), the magnetic field can be presented as

$$\mathbf{B}_{\text{cylinder}} = (B_x, B_y, B_z) = f_c(x, y, z). \tag{18}$$

Then, the solution of the magnetic field generated by an annular magnet using the superposition principle will be

$$\begin{aligned}\mathbf{B}_{\text{annular}} &= f_{\text{annular}}(x, y, z) \\ &= f_c(x, y, z, r_1) - f_c(x, y, z, r_2)\end{aligned} \tag{19}$$

where r_1 is the outer radius and r_2 is the inner radius.

B. Comparison Between Two Magnetic Models and Finite Element Analysis Result

The magnetic dipole model can also be used to calculate the magnetic field. Fig. 4 shows the magnetic dipole model. (x_d, y_d, z_d) are the positional parameters of the magnet, $\mathbf{H_0} = (m, n, p)$ is the direction of magnetic moment and $m^2 + n^2 + p^2 = 1$. At position (x_l, y_l, z_l), the magnetic field can be calculated as

$$\mathbf{B}_l^D = B_T \left(\frac{3(\mathbf{H}_0 \cdot \mathbf{P}_l) \times \mathbf{P}_l}{R_l^5} - \frac{\mathbf{H}_0}{R_l^3} \right) \tag{20}$$

where B_T is a constant value related to the size and material of the magnet and

$$\begin{aligned}\mathbf{P}_l &= (x_l - x_d, y_l - y_d, z_l - z_d) \\ R_l &= \sqrt{(x_l - x_d)^2 + (y_l - y_d)^2 + (z_l - z_d)^2}.\end{aligned}$$

To validate the proposed analytical model, a finite element analysis software (Ansoft Maxwell) is used to

$$\begin{aligned} f_y(z_0) = K\,(z - z_0) \Bigg(& \frac{x + a}{\left[\left(y - \sqrt{r^2 - z_0^2}\right)^2 + (z - z_0)^2\right]\left[(x + a)^2 + (z - z_0)^2 + \left(y - \sqrt{r^2 - z_0^2}\right)^2\right]^{\frac{1}{2}}} \\ & - \frac{x - a}{\left[\left(y - \sqrt{r^2 - z_0^2}\right)^2 + (z - z_0)^2\right]\left[(x - a)^2 + (z - z_0)^2 + \left(y - \sqrt{r^2 - z_0^2}\right)^2\right]^{\frac{1}{2}}} \\ & - \frac{x + a}{\left[\left(y + \sqrt{r^2 - z_0^2}\right)^2 + (z - z_0)^2\right]\left[(x + a)^2 + (z - z_0)^2 + \left(y + \sqrt{r^2 - z_0^2}\right)^2\right]^{\frac{1}{2}}} \\ & + \frac{x - a}{\left[\left(y + \sqrt{r^2 - z_0^2}\right)^2 + (z - z_0)^2\right]\left[(x - a)^2 + (z - z_0)^2 + \left(y + \sqrt{r^2 - z_0^2}\right)^2\right]^{\frac{1}{2}}} \Bigg) \end{aligned} \tag{16}$$

$$\begin{aligned} f_z(z_0) = K \Bigg(& \frac{\left(y + \sqrt{r^2 - z_0^2}\right) X}{\left[\left(y + \sqrt{r^2 - z_0^2}\right)^2 + (z - z_0)^2\right]\left[X^2 + \left(y + \sqrt{r^2 - z_0^2}\right)^2 + (z - z_0)^2\right]^{1/2}} \Bigg|_{x-a}^{x+a} \\ & - \frac{\left(y - \sqrt{r^2 - z_0^2}\right) X}{\left[\left(y - \sqrt{r^2 - z_0^2}\right)^2 + (z - z_0)^2\right]\left[X^2 + \left(y - \sqrt{r^2 - z_0^2}\right)^2 + (z - z_0)^2\right]^{1/2}} \Bigg|_{x-a}^{x+a} \\ & + \frac{-(x - a)\,Y}{\left[(x - a)^2 + (z - z_0)^2\right]\left[(x - a)^2 + Y^2 + (z - z_0)^2\right]^{1/2}} \Bigg|_{y-y'}^{y+y'} \\ & + \frac{(x + a)\,Y}{\left[(x + a)^2 + (z - z_0)^2\right]\left[(x + a)^2 + Y^2 + (z - z_0)^2\right]^{1/2}} \Bigg|_{y-y'}^{y+y'} \Bigg) \end{aligned} \tag{17}$$

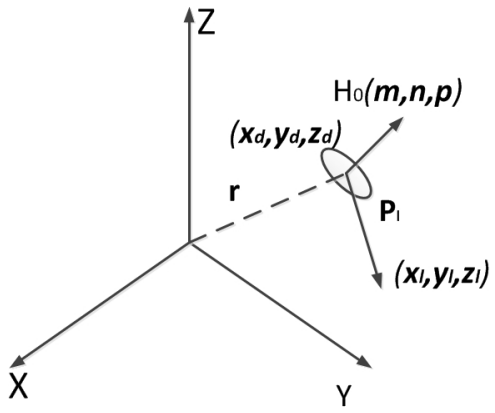

Fig. 4. Magnetic dipole model.

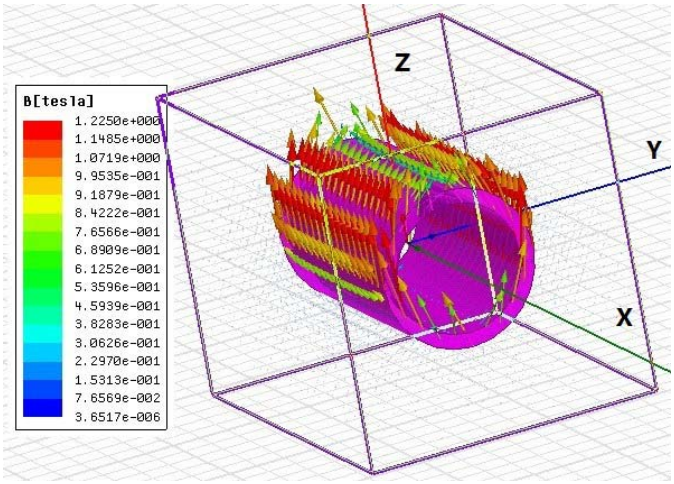

Fig. 5. Simulation result in Ansoft Maxwell.

simulate an annular magnet with size parameters $(a, r_1, r_2) = (9, 5.5, 4.5)$ mm, where a is the half length of the magnet, r_1 is the outer radius, and r_2 is the inner radius. The simulation result is shown in Fig. 5. The coordinate system is based on the annular magnet, so the position and orientation of the dipole model in the local coordinate system should be $(x_d, y_d, z_d) = (0, 0, 0)$ and $(m, n, p) = (0, 0, 1)$. The constant B_T in the magnetic dipole model and K in the annular model can be calculated based on the material and size of the magnet. In Ansoft Maxwell, we chose NdFe35 as the magnetic material, with its relative permeability being 1.0997785406 and magnitude being 890 000 A/m. Defining V_m as the volume of the annular magnet, K and B_T can be calculated as

$$K = \mu_0 \mu_r M / 4\pi = 0.09788$$
$$B_T = K V_m = 5.535e - 8.$$

The comparison points are chosen on a yz plane, where y starts from -6 to 6 mm with a step increment of 2 mm, z starts from -6 to 6 mm with a step increment of 2 mm, and $x = 9.1$ mm. The comparison of the results can be seen in Fig. 6, with the result using the annular magnetic model being represented by the red line, the Ansoft result being represented by the green line and the magnetic dipole model result being represented by the blue line. From Fig. 6, we can see that the annular magnetic model is better than the magnetic dipole model.

Fig. 7 shows the comparison between the results using the annular magnetic model and the magnetic dipole model. Comparison points lie on a space line $(x, y, z) = (t, 1.5t, 0.5t)$ mm $+ (5, 5, 5)$ mm, where t starts from 1 to 10 mm with a step increment of 1 mm. The magnetic field strength B in the figure is defined as

$$B = \sqrt{B_x^2 + B_y^2 + B_z^2}. \tag{21}$$

As an approximate model, the magnetic dipole model works well only when the distance between the sensor and magnet is much larger than the size of the magnet. When the distance is very small, results from the two models are very different. The error between the two models is therefore reduced with increasing distance. Although the values from these two models will converge with increasing distance, the advantage of the proposed model is that the computed values will continuously change during its rotation about the axis of magnetic moment. As shown in Fig. 8, the magnetic field values calculated with these two models at the position $(0.1, 0.15, 0.2)$ m according to the annular magnet's coordinates while the magnet rotates about the z-axis from 0° to 360°. The magnetic dipole model's results (the red line) are constant while the proposed analytical model's results continuously change with the rotation angle. These variations in the values allow the calculation of the rotation angle about the magnetic moment, which cannot be provided by magnetic dipole model.

III. Localization and Orientation Algorithm

The localization algorithm includes two parts: defining a least square problem and solving this problem with an optimization algorithm. We will first define the global localization coordinate system. With this coordinate system, the least square problem for localization and orientation will be introduced. Then particle swarm optimization (PSO) algorithm and an improved fusion method with the magnetic dipole model will be proposed to solve the least square problem.

A. Coordinate System and 6-D Parameters

To realize localization and orientation, a localization coordinate system has to be built. There are two coordinate systems, the global localization coordinate system based on the sensor array, and the local coordinate system based on the annular magnet as shown in Fig. 3. The proposed analytical model in Section II is based on the local coordinate system and the 6-D localization and orientation parameters of the magnet in the global coordinate system are determined by the translation and rotation relationship between the local coordinate system and the global coordinate system.

As shown in Fig. 9, we define the 6-D parameters as $(x_m, y_m, z_m, \alpha, \beta, \gamma)$. (x_m, y_m, z_m) is the 3-D position of the magnet in the global coordinate system and (α, β, γ) is the rotation angle about the x-axis, y-axis, and z-axis based

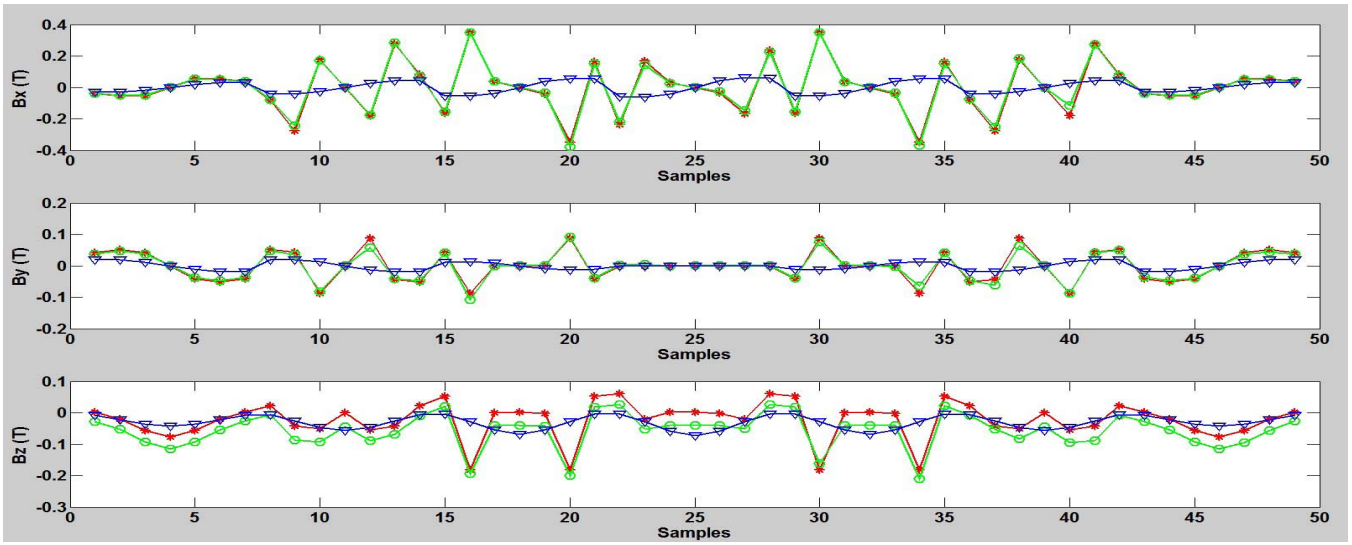

Fig. 6. Comparison result with Ansoft.

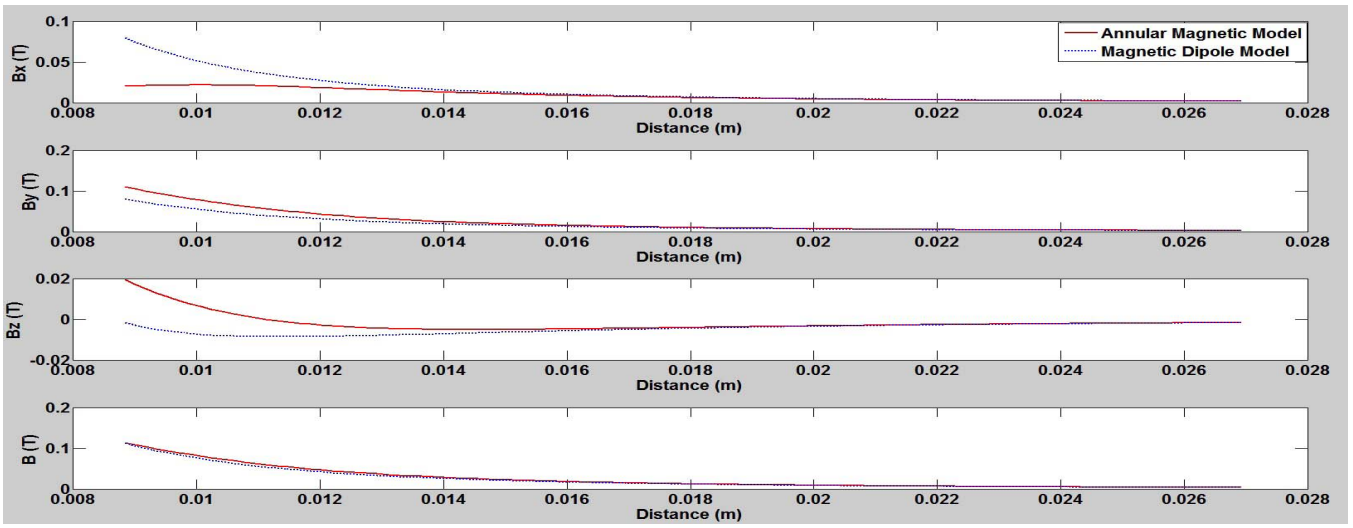

Fig. 7. Comparison result of two models.

on the local coordinate system. The rotation matrix can be decided by

$$\mathbf{R} = \mathrm{Rot}(x, \alpha)\mathrm{Rot}(y, \beta)\mathrm{Rot}(z, \gamma) \tag{22}$$

where

$$\mathrm{Rot}(x, \alpha) = \begin{bmatrix} 1 & 0 & 0 \\ 0 & \cos\alpha & -\sin\alpha \\ 0 & \sin\alpha & \cos\alpha \end{bmatrix}$$

$$\mathrm{Rot}(y, \beta) = \begin{bmatrix} \cos\beta & 0 & \sin\beta \\ 0 & 1 & 0 \\ -\sin\beta & 0 & \cos\beta \end{bmatrix}$$

$$\mathrm{Rot}(z, \gamma) = \begin{bmatrix} \cos\gamma & -\sin\gamma & 0 \\ \sin\gamma & \cos\gamma & 0 \\ 0 & 0 & 1 \end{bmatrix}.$$

B. Localization and Orientation Method

A magnetic sensor array is used to locate the magnet. Each sensor measures the magnetic field strength at its position and outputs three voltages V_x, V_y, and V_z, which indicate the field strength on three orthogonal directions parallel to the global coordinate system axes.

Taking ith sensor as an example: Let its position be $\mathbf{P_i} = (x_i, y_i, z_i)$. The output voltages will be $\mathbf{V_i} = (V_{ix}, V_{iy}, V_{iz})$. Parameters of the magnet are $(x_m, y_m, z_m, \alpha, \beta, \gamma)$. Using (19), the magnetic field value at position $\mathbf{P_i}$ can be calculated as follows:

$$\mathbf{B}_i = f_{\text{annular}}(x_{il}, y_{il}, z_{il})\mathbf{R}^{-1} \tag{23}$$

where

$$(x_{il}, y_{il}, z_{il}) = [(x_i, y_i, z_i) - (x_m, y_m, z_m)]\,\mathbf{R} \tag{24}$$

(x_{il}, y_{il}, z_{il}) is the position of the ith sensor in the local

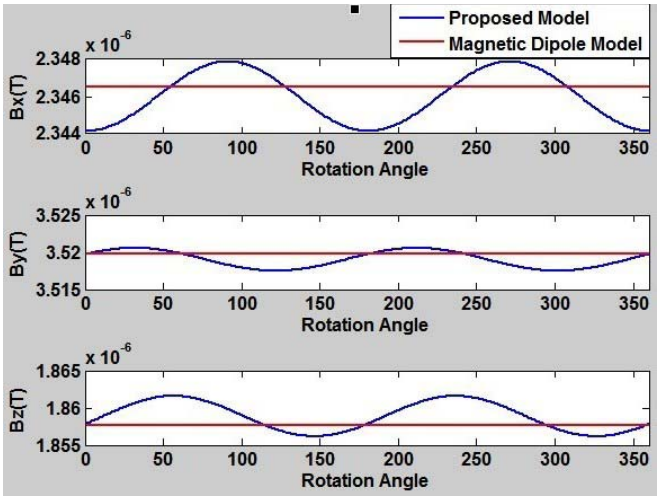

Fig. 8. Comparison result of two models. The magnetic field values are calculated with these two models at the position (0.1, 0.15, 0.2) m in the annular magnet coordinate while the magnet rotating about z-axis from 0° to 360°.

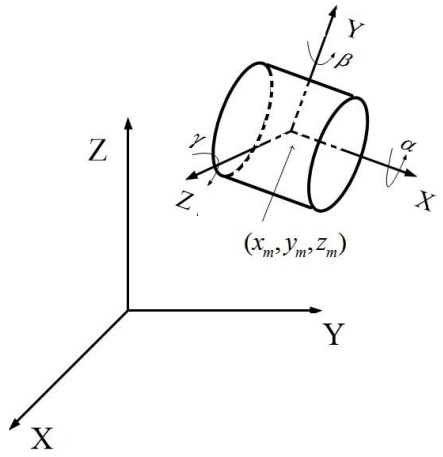

Fig. 9. Localization and orientation parameters.

magnet coordinate system. We define

$$\mathbf{B}_\mathbf{i}' = C_i \cdot \mathbf{V}_\mathbf{i} \tag{25}$$

where C_i is the proportional coefficient between the values of $\mathbf{B_i}$ and $\mathbf{V_i}$. Then, we can have the equation $\mathbf{B_i} = \mathbf{B_i'}$ which contains the unknown parameters $(x_m, y_m, z_m, \alpha, \beta, \gamma)$, and $N(\geq 6)$ equations can be used to solve for the parameters. An effective optimization algorithm is needed to solve these parameters as the equations are so complex that ordinary methods cannot be used here. Defining the error function as

$$\text{Err} = \sum_{i=1}^{N} \parallel \mathbf{B_i} - \mathbf{B_i'} \parallel^2 . \tag{26}$$

The result can be obtained by minimizing Err using an effective optimization algorithm, which will be introduced in the subsequent section.

C. Optimization Algorithm

Equation (26) is a least square error problem; it can be solved using an optimization method. Many effective optimization algorithms can achieve high-quality performance, such as the Levenberg–Marquardt (LM) algorithm, Gauss–Newton (GN) algorithm, Genetic algorithm (GA), PSO algorithm, and so on. As the analytical model is based on a numerically evaluate integral method, the PSO algorithm is used here to solve this problem.

The PSO is a population-based stochastic optimization technique inspired by the social behavior of bird flocking or fish schooling [40]. For the $(t+1)$th time iteration, all particles update their positions by the following equations:

$$V_i(t+1) = \omega \times V_i(t) + c_1 \times a_1 \times (P_i - X_i(t)) + c_2 \times a_2 \times (P_g - X_i(t)) \tag{27}$$

$$X_i(t+1) = X_i(t) + V_i(t+1) \tag{28}$$

where ω is inertia weight, c_1 and c_2 are acceleration constants, a_1 and a_2 are random values between 0 and 1, respectively, P_i is the local optimal result of particles X_i, and P_g is the current global optimal result.

The advantage of the PSO algorithm is that the continuity of the fitness function is not necessary, so it is particularly fitting for the expression of the magnetic model which is based on the numerically evaluate integral method. The shortcoming of this algorithm is that when the fitness function is very complex, there will be many local minimum solutions and a larger population size is needed, which will greatly slow down the speed. A large boundary range would also give rise to more inaccurate results. To get more accurate results, a larger population size and more iterations are needed, which leads to a much slower speed. Since the fitness function cannot be simplified, an effective way to address the speed problem is to limit the boundary range, which will be discussed in the following part.

D. Fusion of the Annular Magnetic Model and Magnetic Dipole Model

To solve the problems with PSO, we combine the two magnetic models together. First, the magnetic dipole model is used to calculate the 5-D parameters, and then the boundaries in the PSO algorithm are set based on the 5-D result. Subsequently, the PSO algorithm is carried out. The detailed steps are as follows.

1) Magnetic Dipole Model: We integrate the dipole model into the localization system, and define the parameters of magnetic dipole model as (x_d, y_d, z_d, m, n, p). (x_d, y_d, z_d) is the magnet position in the global coordinate system, while (m, n, p) is the magnetic orientation in the global coordinate system.

Define the error evaluation function of the magnetic dipole model as

$$Err_{\text{dipole}} = \sum_{i=1}^{N} \parallel \mathbf{B}_i^D - \mathbf{B_i'} \parallel^2 \tag{29}$$

where $\mathbf{B}_i'$ is defined in (25) and $\mathbf{B}_i^D$ is the result obtained using the magnetic dipole model. Then (x_d, y_d, z_d, m, n, p) can be solved with the LM algorithm [26].

2) Parameters Transform: The position (x_d, y_d, z_d) can serve as the initial value for (x_m, y_m, z_m). The direction (m, n, p) can provide two rotation angles α and β. The relationship between (m, n, p) and (α, β, γ) is as follows:

$$(m, n, p)\mathbf{R} = (0, 0, 1) \tag{30}$$

that is

$$(m, n, p) = (\sin\beta, -\sin\alpha\cos\beta, \cos\alpha\cos\beta) \tag{31}$$

then α and β can be solved.

3) PSO Algorithm: Using the above results as the initial value of $(x_m, y_m, z_m, \alpha, \beta)$, the bound in PSO can be set as

$$\text{Bound}_{(x,y,z,\alpha,\beta,\gamma)} = \left(x_m, y_m, z_m, \alpha, \beta, \frac{\pi}{2}\right) \pm \left(\Delta x_m, \Delta y_m, \Delta z_m, \Delta\alpha, \Delta\beta, \frac{\pi}{2}\right) \tag{32}$$

where Δx_m, Δy_m, Δz_m, $\Delta\alpha$, and $\Delta\beta$ are very small values decided by the accuracy of the magnetic dipole model. By setting bounds in a very small space, the populations and iterations can be reduced, while maintaining the accuracy.

IV. Simulation Results

A. Example

The purpose of the simulations is to test the solvability of the magnetic model and the PSO algorithm. First, an example will be shown to illustrate how the proposed analytical model and simulation work. The assumed simulation workspace is inside the sensor array as shown in Fig. 1. The global localization coordinate system is built on the bottom plane of the array. Position and orientation parameters of the magnet in the sensor array are set as

$$(x_m, y_m, z_m, \alpha, \beta, \gamma) = \left(0.1\text{ m}, 0.2\text{ m}, 0.22\text{ m}, \frac{\pi}{3}, \frac{\pi}{4}, \frac{\pi}{6}\right).$$

Then the magnetic field strength at each sensor position can be calculated using (23). For example, at position (0.128, −0.244, 0.307 m), the calculated results is

$$\begin{cases} B_x = -0.341681154884478 \times 10^{-6}\text{ T} \\ B_y = -0.878337978247516 \times 10^{-6}\text{ T} \\ B_z = \ 0.0333900132524796 \times 10^{-6}\text{ T}. \end{cases}$$

The sensors' position information are based on the sensor array as shown in Fig. 1. In the example and the following simulation, a total of 36 magnetic sensors is used to calculate magnetic field strength. The parameters of the annular magnet are the same as the parameters used in the comparison part. Also, no noise signals are added in the simulation, as the purpose of the simulation is to test and verify the feasibility and solvability of the analytical model.

With the magnetic field strength data, the magnetic dipole model can be used to solve for the position and orientation parameters. Here, the LM algorithm is used and the result is

$$(x_d, y_d, z_d, m, n, p) = (0.1002, 0.2002, 0.2201, 0.7067, -0.6143, 0.3518).$$

TABLE I
Calculation Time Comparison Between LM and PSO

Algorithm	Calculation Time
LM	0.08s
PSO	830s

TABLE II
Accuracy of PSO Fusion With LM and Without LM

	PSO without LM	PSO with LM	Ground Truth
x	0.1003m	0.1m	0.1m
y	0.2001m	0.2m	0.2m
z	0.2199m	0.22m	0.22m
α	60.0885°	60.0002°	60°
β	45.0040°	44.9998°	45°
γ	66.8485°	29.9975°	30°

Convert (m, n, p) to (α, β)

$$(\alpha, \beta) = (1.0507(60.20°),\ 0.7848(44.97°)).$$

As an approximate model, we can see that the magnetic dipole model result is much closer to the real result. Then, setting $(\Delta x_m, \Delta y_m, \Delta z_m, \Delta\alpha, \Delta\beta)$ as (0.001, 0.001, 0.001, 0.01, 0.01) and using the PSO algorithm to calculate the annular magnetic model, we have

$$(x_m, y_m, z_m, \alpha, \beta, \gamma) = (0.1,\ 0.2,\ 0.22,\ 1.0472,\ 0.7854,\ 0.5236).$$

Converting (α, β, γ) to degrees, we obtain

$$(\alpha, \beta, \gamma) = (60.0002°,\ 44.9998°,\ 29.9975°).$$

As mentioned before, the PSO algorithm is much slower than the LM algorithm. Table I shows the comparisons between calculation times. Here, the population parameter of PSO is set to 2000 and iteration time is set to 50. The calculation is then run in MATLAB on a PC with an i7-2600 CPU and 8G RAM. It can be seen that the PSO algorithm is much slower due to the large population value. We hope to improve this in future.

With the same setting of PSO, the comparison between the results of PSO by establishing the initial bounds without LM and with LM is shown in Table II. We can see that the accuracy of the localization result from using PSO with LM is better than the result of using PSO without LM, especially for γ.

B. Simulation

First position error and orientation error are defined as E_p and E_o, respectively

$$E_p = \sqrt{(x_r - x_c)^2 + (y_r - y_c)^2 + (z_r - z_c)^2} \tag{33}$$

$$E_o = (|\ \alpha_r - \alpha_c\ | + |\ \beta_r - \beta_c\ | + |\ \gamma_r - \gamma_c\ |) \tag{34}$$

where $(x_r, y_r, z_r, \alpha_r, \beta_r, \gamma_r)$ is the ground truth and $(x_c, y_c, z_c, \alpha_c, \beta_c, \gamma_c)$ is the estimated value.

As shown in Fig. 10, 30 random positions inside the sensor array (Fig. 1) with random rotation angles have been tested in the simulation. These random positions are distributed in a space of 0.36 m × 0.37 m × 0.3 m.

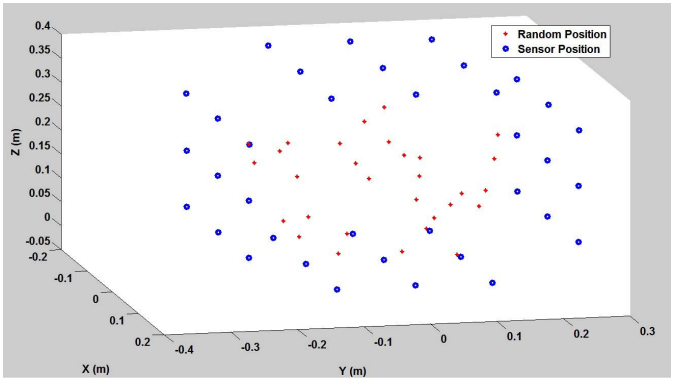

Fig. 10. Simulation points and sensors' position. Blue points: sensors' position. Red points: 30 random test positions.

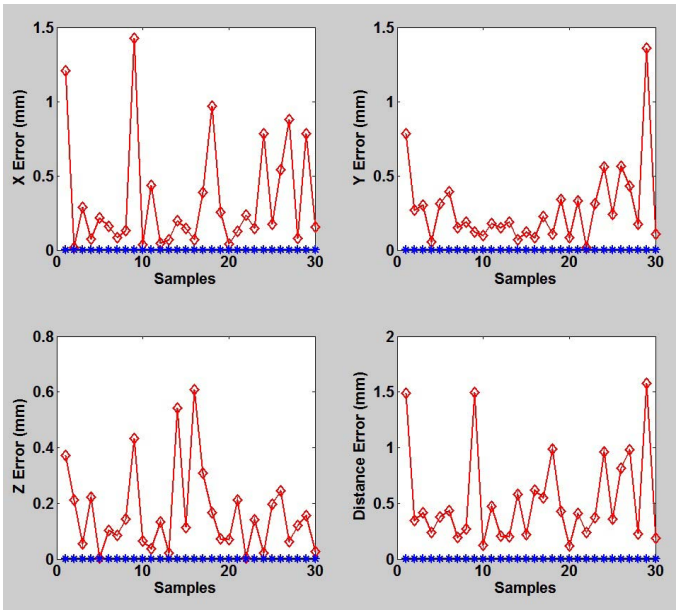

Fig. 11. Position error. Red points: result from magnetic dipole model. Blue stars: result from the annular magnetic model.

Fig. 11 shows the position errors, where red points represent the result from the magnetic dipole model and blue stars represent the result from the annular magnetic model. The average position error of the magnetic dipole model is 0.5 mm and the average error of the annular magnetic model is 0.003 mm. From the results we can see that the magnetic dipole model is a good approximation model and it can be used in many applications that do not need 6-D information or high accuracy. The annular magnetic model can solve this problem and achieve a very high accuracy.

Fig. 12 shows the orientation errors, where the red line represents the result from the magnetic dipole model and blue stars represent the result from the annular magnetic model. The final average orientation error of the annular model is 0.036°. We can see that the errors on α and β are very small, but the error on γ is a little bigger. This is because α and β are estimated based on the initial value from the magnetic dipole model, while there is no initial value for γ, but only a bound

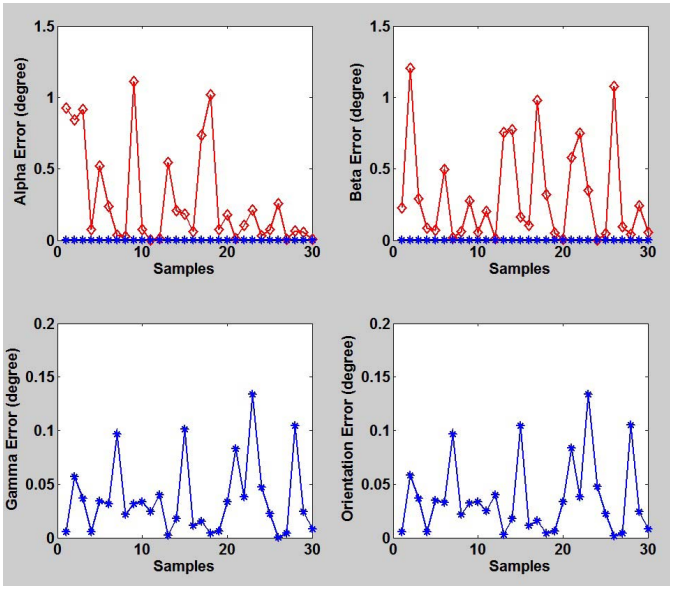

Fig. 12. Orientation error. Red points: result from magnetic dipole model. Blue stars: result from the annular magnetic model.

area to search from. With many local optimal solutions around the true value, it is difficult for the accuracy of γ to be as good as α and β.

Note that no noise is added in the simulation experiments, so the accuracy is very high and the solvability of this proposed model has been verified.

V. Conclusion

A new 6-D localization and orientation method for a wireless capsule endoscope have been presented and discussed based on an annular permanent magnet. A novel closed-form analytical model for the annular magnet is proposed and the PSO algorithm is used to implement the optimization. Extensive simulation results show that this method works well and the accuracy is very high. The optimization time is now very large and we will simplify the expression and make this method work in real time in the future. In terms of applications, the proposed approach can be used to track miniature intracorporeal instruments, such as the tips of conventional flexible endoscopes and wireless capsule endoscopes, which is an emerging technology to view the small intestine without discomfort. This will allow physicians to know the exact position and orientation of medical instruments inside human body.

VI. Acknowledgment

This work was supported in part by the National Natural Science Foundation of China under Grant 61273332 and 61305099, in part by the Singapore Academic Research Fund under Grant R397000139133, Grant R397000157112, Grant R397000156112, and Grant R397000173133, and in part by the National University of Singapore under Grant C397000043511.

REFERENCES

[1] H. Ren *et al.*, "Computer assisted transoral surgery with flexible robotics and navigation technologies: A review of recent progress and research challenges," *Critical Rev. Biomed. Eng.*, vol. 41, nos. 4–5, pp. 365–391, 2013.

[2] S. Vincent, D. Predrag, R. S. Popovic, and K. Pavel, "A magnetic tracking system based on highly sensitive integrated Hall sensors," *JSME Int. J. Ser. C, Mech. Syst., Mach. Elements Manuf.*, vol. 45, no. 4, pp. 967–973, 2002.

[3] C. Hu, M. Li, S. Song, R. Zhang, M.-H. Meng, and W. Yang, "A cubic 3-axis magnetic sensor array for wirelessly tracking magnet position and orientation," *IEEE Sensors J.*, vol. 10, no. 5, pp. 903–913, May 2010.

[4] W. Weitschies, M. Karaus, D. Cordini, L. Trahms, J. Breitkreutz, and W. Semmler, "Magnetic marker monitoring of disintegrating capsules," *Eur. J. Pharmaceutical Sci.*, vol. 13, no. 4, pp. 411–416, 2001.

[5] H. Ren, W. Lim, and W. Guo, "Coverage planning in computer-assisted ablation based on genetic optimization," *Comput. Biol. Med.*, vol. 49C, pp. 36–45, Mar. 2014.

[6] H. Ren and X. Kang, "Surgical navigation and planning with minimum radiation in orthopaedic interventions," in *Proc. 13th Annu. Meeting Int. Society CAOS*, Orlando, FL, USA, Jun. 2013.

[7] H. Ren, W. Liu, and S. Song, "Towards occlusion-resistant surgical instrument tracking," *Bone Joint J. Orthopaedic Proc. Suppl.*, vol. 95-B, no. 28, p. 52, 2013.

[8] H. Ren, E. Campos-Nanez, Z. Yaniv, F. Banovac, N. Hata, and K. Cleary, "Treatment planning and image guidance for radiofrequency ablations of large tumors," *IEEE J. Biomed. Health Inform.*, vol. 18, no. 3, pp. 920–928, 2014.

[9] H. Ren, W. Liu, and A. Lim, "Marker-based instrument tracking using dual kinect sensors for navigated surgery," *IEEE Trans. Autom. Sci. Eng.*, vol. 11, no. 3, pp. 921–924, 2014.

[10] A. Hamed *et al.*, "Advances in haptics, tactile sensing, and manipulation for robot-assisted minimally invasive surgery, noninvasive surgery, and diagnosis," *J. Robot.*, vol. 2012, p. 412816-1–412816-14, Jan. 2012.

[11] H. Ren and P. Kazanzides, "Investigation of attitude tracking using an integrated inertial and magnetic navigation system for hand-held surgical instruments," *IEEE/ASME Trans. Mechatronics*, vol. 17, no. 2, pp. 210–217, Apr. 2012.

[12] H. Ren, R. Denis, M. Martin, S. Jan, and P. Kazanzides, "Multi-sensor data fusion in an integrated tracking system for endoscopic surgery," *IEEE/ASME Trans. Inform. Technol. Biomed.*, vol. 16, no. 1, pp. 106–111, Jan. 2012.

[13] J. Stoll, H. Ren, and P. E. Dupont, "Passive markers for tracking surgical instruments in real-time 3-D ultrasound imaging," *IEEE Trans. Med. Imag.*, vol. 31, no. 3, pp. 563–575, Mar. 2012.

[14] H. Ren and P. Kazanzides, "A paired-orientation alignment problem in a hybrid tracking system for computer assisted surgery," *J. Intell. Robot. Syst.*, vol. 63, no. 2, pp. 151–161, 2011.

[15] H. Ren and M. Q.-H. Meng, "Game-theoretic modeling of joint topology control and power scheduling for wireless heterogeneous sensor networks," *IEEE Trans. Autom. Sci. Eng.*, vol. 6, no. 4, pp. 610–625, Oct. 2009.

[16] H. Ren and M. Q.-H. Meng, "Power adaptive localization algorithm for wireless sensor networks using particle filter," *IEEE Trans. Veh. Technol.*, vol. 58, no. 5, pp. 2498–2508, Jun. 2009.

[17] M.-H. Meng, T. Mei, J. Pu, C. Hu, X. Wang, and Y. Chan, "Wireless robotic capsule endoscopy: State-of-the-art and challenges," in *Proc. 5th WCICA*, vol. 6. Jun. 2004, pp. 5561–5565.

[18] C. Hu, M. Q.-H. Meng, and M. Mandal, "The calibration of 3-axis magnetic sensor array system for tracking wireless capsule endoscope," in *Proc. IEEE/RSJ Int. Conf. Intelligent Robots and Systems*, Oct. 2006, pp. 162–167.

[19] F. Carpi and C. Pappone, "Magnetic maneuvering of endoscopic capsules by means of a robotic navigation system," *IEEE Trans. Biomed. Eng.*, vol. 56, no. 5, pp. 1482–1490, May 2009.

[20] E. Paperno, I. Sasada, and E. Leonovich, "A new method for magnetic position and orientation tracking," *IEEE Trans. Magn.*, vol. 37, no. 4, pp. 1938–1940, Jul. 2001.

[21] A. Plotkin, E. Paperno, G. Vasserman, and R. Segev, "Magnetic tracking of eye motion in small, fast-moving animals," *IEEE Trans. Magn.*, vol. 44, no. 11, pp. 4492–4495, Nov. 2008.

[22] C. Hu, S. Song, X. Wang, M.-H. Meng, and B. Li, "A novel positioning and orientation system based on three-axis magnetic coils," *IEEE Trans. Magn.*, vol. 48, no. 7, pp. 2211–2219, Jul. 2012.

[23] S. Song, C. Hu, B. Li, X. Li, and M.-H. Meng, "An electromagnetic localization and orientation method based on rotating magnetic dipole," *IEEE Trans. Magn.*, vol. 49, no. 3, pp. 1274–1277, Mar. 2013.

[24] S. Song, W. Qiao, B. Li, C. Hu, H. Ren, and M.-H. Meng, "An efficient magnetic tracking method using uniaxial sensing coil," *IEEE Trans. Magn.*, vol. 50, no. 1, pp. 1–7, Jan. 2014.

[25] C. Hu, M.-H. Meng, S. Song, H. Dai, and W. Yang, "A six-dimensional magnetic localization algorithm for a rectangular magnet objective based on a particle swarm optimizer," *IEEE Trans. Magn.*, vol. 45, no. 8, pp. 3092–3099, Aug. 2009.

[26] S. Song, C. Hu, M. Li, W. Yang, and M.-H. Meng, "Real time algorithm for magnet's localization in capsule endoscope," in *Proc. IEEE ICAL*, Aug. 2009, pp. 2030–2035.

[27] X. Wu, W. Hou, C. Peng, X. Zheng, X. Fang, and J. He, "Wearable magnetic locating and tracking system for MEMS medical capsule," *Sens. Actuators A, Phys.*, vol. 141, no. 2, pp. 432–439, 2008.

[28] W. Yang, Y. Li, C. Hu, and S. Song, "A real-time tracking method for the rectangular magnet based on parallel Levenberg–Marquardt algorithm," *Int. J. Appl. Electromagn. Mech.*, vol. 37, no. 4, pp. 241–251, 2011.

[29] S. Song, C. Hu, M. Li, W. Yang, and M.-H. Meng, "Two-magnet-based 6D-localization and orientation for wireless capsule endoscope," in *Proc. IEEE Int. Conf. Robotics and Biomimetics*, Dec. 2009, pp. 2338–2343.

[30] X. Chen, S. Tamura, D. Lin, and Y. Du, "A 3D localization and navigation method for endoscope by magnetic field," *J. Comput. Res. Develop.*, vol. 39, no. 2, pp. 325–329, 2002.

[31] M. Sendoh, K. Ishiyama, and K.-I. Arai, "Fabrication of magnetic actuator for use in a capsule endoscope," *IEEE Trans. Magn.*, vol. 39, no. 5, pp. 3232–3234, Sep. 2003.

[32] X. Guo, G. Yan, W. He, and P. Jiang, "Improved modeling of electromagnetic localization for implantable wireless capsules," *J. Inform.*, vol. 44, no. 4, pp. 354–359, 2010.

[33] H. Ren and P. Kazanzides, "Hybrid attitude estimation for laparoscopic surgical tools: A preliminary study," in *Proc. Annu. Int. Conf. IEEE Engineering Medicine and Biology Society*, Sep. 2009, pp. 5583–5586.

[34] K. Enpuku, D. Kuroda, T. Yang, and K. Yoshinaga, "High T_c SQUID system and magnetic marker for biological immunoassays," *IEEE Trans. Appl. Supercond.*, vol. 13, no. 2, pp. 371–376, Jun. 2003.

[35] V. Schlageter, P.-A. Besse, R. Popovic, and P. Kucera, "Tracking system with five degrees of freedom using a 2D-array of Hall sensors and a permanent magnet," *Sens. Actuators A, Phys.*, vol. 92, no. 1, pp. 37–42, 2001.

[36] M. Birsan, "Recursive Bayesian method for magnetic dipole tracking with a tensor gradiometer," *IEEE Trans. Magn.*, vol. 47, no. 2, pp. 409–415, Feb. 2011.

[37] W.-S. Yao, M.-C. Tsai, J.-Z. Lai, and F.-Y. Yang, "Detection of magnetic object movements by flux density tracking control," *IEEE/ASME Trans. Mechatronics*, vol. 17, no. 4, pp. 709–716, Aug. 2012.

[38] M. Katie, W. Arthur, and J. Jake, "Localization method for a magnetic capsule endoscope propelled by a rotating magnetic dipole field," in *Proc. IEEE ICRA*, May 2013, pp. 5328–5333.

[39] C. Di Natali, M. Beccani, and P. Valdastri, "Real-time pose detection for magnetic medical devices," *IEEE Trans. Magn.*, vol. 49, no. 7, pp. 3524–3527, Jul. 2013.

[40] R. Eberhart and J. Kennedy, "A new optimizer using particle swarm theory," in *Proc. 6th Int. Symp. MHS*, Oct. 1995, pp. 39–43.